

Volatility of Secondary Organic Aerosol from β -Caryophyllene Ozonolysis over a Wide Tropospheric Temperature Range

Linyu Gao,* Angela Buchholz, Zijun Li, Junwei Song, Magdalena Vallon, Feng Jiang, Ottmar Möhler, Thomas Leisner, and Harald Saathoff*



Cite This: *Environ. Sci. Technol.* 2023, 57, 8965–8974



Read Online

ACCESS |



Metrics & More



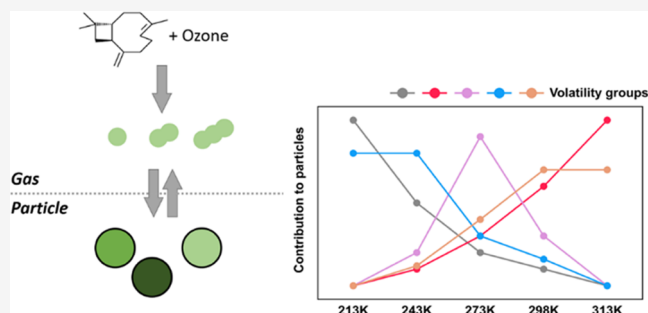
Article Recommendations



Supporting Information

ABSTRACT: We investigated secondary organic aerosol (SOA) from β -caryophyllene oxidation generated over a wide tropospheric temperature range (213–313 K) from ozonolysis. Positive matrix factorization (PMF) was used to deconvolute the desorption data (thermograms) of SOA products detected by a chemical ionization mass spectrometer (FIGAERO-CIMS). A nonmonotonic dependence of particle volatility (saturation concentration at 298 K, C_{298K}^*) on formation temperature (213–313 K) was observed, primarily due to temperature-dependent formation pathways of β -caryophyllene oxidation products. The PMF analysis grouped detected ions into 11 compound groups (factors) with characteristic volatility. These compound groups act as indicators for the underlying SOA formation mechanisms. Their different temperature responses revealed that the relevant chemical pathways (e.g., autoxidation, oligomer formation, and isomer formation) had distinct optimal temperatures between 213 and 313 K, significantly beyond the effect of temperature-dependent partitioning. Furthermore, PMF-resolved volatility groups were compared with volatility basis set (VBS) distributions based on different vapor pressure estimation methods. The variation of the volatilities predicted by different methods is affected by highly oxygenated molecules, isomers, and thermal decomposition of oligomers with long carbon chains. This work distinguishes multiple isomers and identifies compound groups of varying volatilities, providing new insights into the temperature-dependent formation mechanisms of β -caryophyllene-derived SOA particles.

KEYWORDS: volatility, secondary organic aerosol (SOA), positive matrix factorization (PMF), β -caryophyllene, temperature dependence



INTRODUCTION

Secondary organic aerosol (SOA) has adverse effects on air quality, human health, and the climate.^{1–4} Oxidation products of biogenic volatile organic compounds (BVOCs) are the main contributors to SOA mass by gas-to-particle partitioning after their oxidation in the gas phase.^{5–7} Volatility is a key physicochemical property determining the condensation and evaporation of, e.g., organic compounds. Thus, volatility determines the atmospheric fate of organic molecules and is important for understanding SOA formation and growth.⁸

However, it still remains unclear how environmental temperature impacts the formation of biogenic SOA particles in the atmosphere. Reduced temperatures lower the saturation vapor pressures (V_p) of compounds according to the Clausius–Clapeyron relation, which would drive organic compounds into the particle phase.⁸ On the other hand, it was found that for the ozonolysis of α -pinene^{9,10} and β -caryophyllene,¹¹ higher temperatures strongly affect gas-phase unimolecular reaction rates and increase the generation of more oxidized compounds with lower V_p .⁶ Thus, the temperature can have opposite impacts on the condensation of less oxidized compounds and the formation of highly

oxygenated organic molecules (HOMs). The interplay between these two aspects increases the complexity of SOA formation and complicates the predictions of particle volatility in different seasons and/or altitudes.¹²

Currently, the mostly used method to derive the volatility of organic compounds from mass spectrometry data is the parameterization of the detected elemental formulas.^{13–15} Parameterization methods omit the existence of isomers, i.e., one volatility value is assigned for each elemental formula, while volatilities of isomers may vary by orders of magnitude owing to their different functionalities and molecular structures.^{16,17} For the chemical ionization time-of-flight mass spectrometer (TOFMS) with filter inlet for gases and AEROSols (FIGAERO-CIMS) measurements, the thermal desorption behavior (thermograms) of the detected ions

Received: February 10, 2023

Revised: May 6, 2023

Accepted: May 15, 2023

Published: June 7, 2023



correlates with their V_p . If an elemental formula represents only one compound, the thermogram would be monomodal and the T_{\max} value directly relates to its V_p .^{18,19} If multiple isomers are present and/or other compounds thermally decompose to this sum formula, multiple modes may be observed and a single T_{\max} is no longer representative for the overall volatility.^{18,20} A newly extended approach based on positive matrix factorization (PMF) analysis^{13,21} helps us to distinguish isomers and thermal decomposition compounds in mass spectrometry data by deconvoluting the thermal desorption profiles of ions.

Recently, sesquiterpenes ($C_{15}H_{24}$) have gained more attention due to their importance in contributing to the overall SOA mass yield from, e.g., Scots pine emissions and the potential underestimation of their contribution to the global SOA mass.^{22–29} A recent modeling study showed that the global SOA burden can be enhanced by 48% relative to the base case when including sesquiterpenes into the model.³⁰ β -Caryophyllene has the largest emissions among all bicyclic sesquiterpenes, which retain their large carbon chains throughout the oxidation process, and thus it acts as the proxy of sesquiterpenes in modeling studies on the estimation of global biogenic SOA mass.^{31,32} Due to its high reactivity toward ozone^{33,34} and low volatilities of its oxidation products, such as its atmospheric tracer β -caryophyllinic acid ($C_{14}H_{22}O_4$),³⁵ β -caryophyllene plays an important role in SOA formation and particle growth in local cases.^{22,25,36,37} Strong temperature dependence was found in the chemical composition of SOA from β -caryophyllene oxidation with abundant dimers/oligomers (e.g., $C_{28–30}H_{44–48}O_{5–9}$ and $C_{41–44}H_{62–66}O_{9–11}$) at 213–243 K and higher oxidized monomers (e.g., $C_{14–15}H_{22–24}O_{3–7}$) at 298–313 K.¹¹ However, to date, there is still a lack of understanding on the interplay between the ozonolysis chemistry and the phase partitioning at different temperatures during the formation of β -caryophyllene SOA. Determining volatilities of many β -caryophyllene oxidation products formed at different temperatures is still challenging.

In this work, we applied PMF to revisit a previously published data set of β -caryophyllene ozonolysis SOA formed between 213 and 313 K¹¹ to derive volatility information and provided indicators of temperature-dependent formation mechanisms as an example for other biogenic SOA. The use of PMF enables us to investigate the varying contributions of dimers/oligomers even if they thermally decompose during the measurements.

EXPERIMENTAL SECTION

Simulation Chamber Experiments. Ozonolysis experiments were performed in the 84.5 m³ aluminum Aerosol Interaction and Dynamics in the Atmosphere (AIDA) simulation chamber at the Karlsruhe Institute of Technology (KIT).^{38,39} The chamber operation, experimental conditions, and instrument setup for the campaign are described in the [Supporting Information](#). Briefly, five β -caryophyllene oxidation experiments were separately conducted in the dark at 213, 243, 273, 298, and 313 K (see [Table S1](#)). The β -caryophyllene (98%, Carl Roth GmbH) concentration injected into the chamber was 1.6 ppbv at 243 K and 8–12 ppbv at 273–313 K. At 213 K, due to strong wall loss effects, β -caryophyllene was lost to the chamber wall before the ozone addition, preventing SOA formation. Thus, to generate particles in quantities comparable to other experiments, more β -caryophyllene was added subsequently after the ozone addition for the experi-

ment at 213 K. Ozone (99.9999%) was typically in excess with concentrations of 290–320 ppb except for the 273 K experiment, where the initial ozone concentration was 73 ppbv. No hydroxyl radical scavenger was used in any experiments. Note that the β -caryophyllene concentration as well as its ratio to ozone varied between individual experiments. However, in all experiments, ozone was in a substantial excess compared to the β -caryophyllene concentration. Thus, the temperature is the dominant influence, e.g., for the formation of oligomers, instead of the varying precursor concentrations.

Particle Measurement. An iodide adduct chemical ionization mass spectrometer (I^- -CIMS) coupled with a Filter Inlet for Gas and AEROSol (FIGAERO)¹⁸ (Aerodyne Research Inc. & ToFwerk AG) was used to analyze the composition and volatility of SOA particles.

The particle data presented in this work stem from offline analysis. Particles were deposited on a Teflon filter (poly(tetrafluorethylene), PTFE, 1 μ m, SKC Inc.) with a collection flow rate of 6.4 L min⁻¹ for typically 5–10 min. Afterward, the collected samples were stored in a freezer (at -30 °C) and then were analyzed by the FIGAERO-CIMS using pure nitrogen (99.9999%, Basi Schöberl GmbH) as a carrier gas. The desorption temperature was ramped linearly from 25 to 200 °C for 15 min and then held near 200 °C for 20 min to ensure the evaporation of most compounds deposited on the filter. Data were collected at 1 Hz and averaged over 10 s for postprocessing. Raw data were analyzed using Tofware v3.1.2. Although the sensitivities of the iodide CIMS toward oxygenated compounds span about three orders of magnitude, we assumed uniform sensitivity for all compounds detected by FIGAERO-CIMS and only used signal intensity for the comparisons presented here. Note that we did not calculate concentrations except for β -caryophyllinic acid for which we were able to determine the sensitivity to be (2.4^{+0.96}_{-0.63}) cps/ppt, while the maximum sensitivity of the iodide CIMS has been determined at 22 cps/ppt.⁴⁰ The limitations of the FIGAERO offline analysis are discussed in the [SI](#).

Before each experiment, the chamber air was sampled and analyzed in the same fashion as the experimental samples to provide the background stemming from the chamber, filter matrix, and instrument. The mass spectra of background filter samples were subtracted from those of particle samples for the same experiments.

Additionally, the bulk chemical composition was monitored with a high-resolution time-of-flight aerosol mass spectrometer (HR-AMS, Aerodyne Research Inc.) in real time. High-resolution analysis of the elemental composition including the oxygen-to-carbon (O/C) and hydrogen-to-carbon (H/C) ratios⁴¹ was done with PIKA 1.20 C.^{42,43}

Deconvolution of Thermograms by Positive Matrix Factorization. The statistical method of PMF^{21,44–46} has recently been extended to study the volatilities of SOA constituents by analyzing the thermograms of individual molecules from FIGAERO-CIMS.^{13–15} Isomeric compounds and products from thermal decomposition of larger compounds that appear with the same molecular composition are grouped by their desorption behavior into PMF factors, which can then be compared between experiments. In this study, we used the constant error (CNerror)¹³ approach, which yielded the most interpretable results. The noise was calculated using the thermal desorption data at the end of the thermogram scans, and the CNerror was multiplied by 4 to improve the

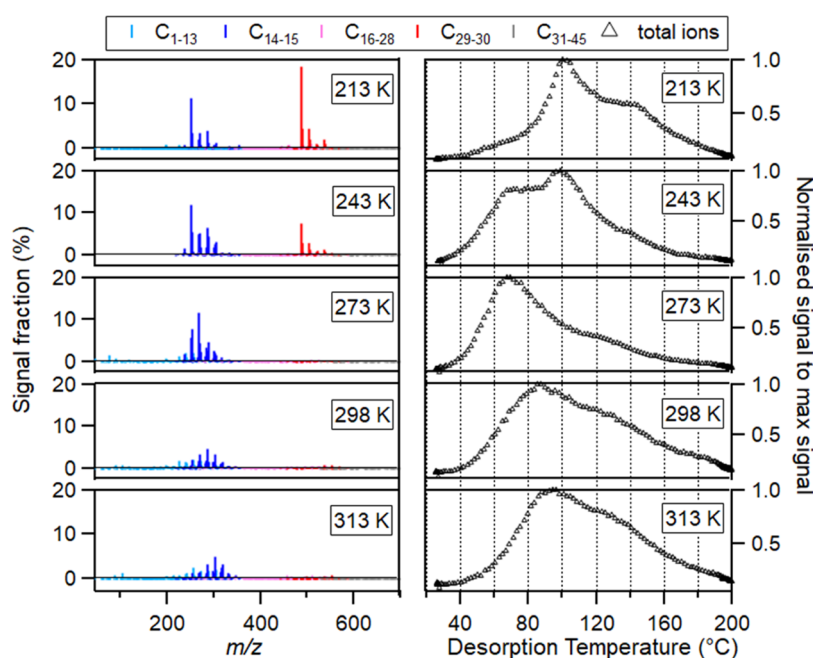


Figure 1. Mass spectra (left) and sum thermogram (right) of SOA (top to bottom) at 213, 243, 273, 298, and 313 K. In the left panel, compounds with different carbon numbers were colored as indicated in the legend. Monomers with 14–15 carbons and dimers with 29–30 carbon atoms are shown with positive values, and other molecules with 1–13 and 16–28 carbon atoms are represented by negative values to enhance readability. Mass spectra are reprinted with permission under the terms of the Creative Commons Attribution 4.0 License.¹¹ Copyright 2022 Gao.

range of Q/Q_{exp} ¹³ values. The PMF analysis was calculated for 1–12 factors with three f_{peak} rotations¹³ from -0.5 to $+0.5$ using the FIGAERO Thermogram PMF Evaluation Tool (FiT PET v1.09 and PET v3.06, Dr. Angela Buchholz, private communication). All five β -caryophyllene SOA experiments were analyzed together and interpreted by the same set of factors. The diagnostics of the selected solution, error scheme, and comparison of different solutions are described in detail in Figures S6 and S7. A background factor (BG1) was identified, covering the remaining instrument background, which was not captured by the chamber blank measurements. The thermograms of $\text{C}_{15}\text{H}_{24}\text{O}_3$ and $\text{C}_{15}\text{H}_{24}\text{O}_4$ were excluded from the PMF analysis and resolved separately, as they have very high signal intensities but were not captured well by the PMF analysis.

Three Volatility Estimation Methods. The volatility of individual compound is here expressed by the saturation concentration at a reference temperature of 298 K ($C_{298\text{K}}^*$, $\mu\text{g m}^{-3}$). The $C_{298\text{K}}^*$ of a compound is related to its V_p as^{47,48}

$$C_{298\text{K}}^* = \frac{V_p \times M_w}{R \times 298\text{ K}} \quad (1)$$

where M_w is the molecular weight of a compound, g mol^{-1} ; R refers to the universal gas constant, $8.314\text{ J K}^{-1}\text{ mol}^{-1}$. The saturation concentration of species at other temperatures (C_T^*) can be derived from $C_{298\text{K}}^*$ according to the Clausius–Clapeyron relation

$$C_T^* = C_{298\text{K}}^* \exp\left(\frac{\Delta H_{\text{vap}}}{R} \left(\frac{1}{298} - \frac{1}{T}\right)\right) \quad (2)$$

where T is the experimental temperature in K; ΔH_{vap} is the evaporation enthalpy in kJ mol^{-1} , which can be estimated by⁴⁹

$$\Delta H_{\text{vap}} = -11 \times \log_{10} C_{298\text{K}}^* + 129 (\text{kJ mol}^{-1}) \quad (3)$$

For comparisons, we use the following volatility classes:^{50,51} ultralow VOC (ULVOC, $\log_{10} C^* < -8.5$, gray), extremely low VOC (ELVOC, $-8.5 < \log_{10} C_{298\text{K}}^* < -4.5$, blue), low VOC (LVOC, $-4.5 < \log_{10} C_{298\text{K}}^* < -0.5$, orange), semi-VOC (SVOC, $-0.5 < \log_{10} C_{298\text{K}}^* < -2.5$, pink), intermediate VOC (IVOC, $2.5 < \log_{10} C_{298\text{K}}^* < 6.5$, green), and VOC ($\log_{10} C_{298\text{K}}^* > 6.5$, yellow). The boundaries of the volatility classes are defined at 298 K and are shifted to the corresponding values at the formation temperatures using the Clausius–Clapeyron relation.¹²

Note that, to avoid any confusion in the description, the word “compound” hereafter refers to one unique constitute, and the word “ion” represents all of the detected isomers behind a common sum formula.

In this work, we used three approaches to determine $C_{298\text{K}}^*$: (1) the measured elemental formulas applying a parameterization using molecular corridors^{8,52} (“formula” method); (2) the correlation between effective vapor pressures and peak desorption temperatures of molecules^{18,19,48,53} (“ T_{max} method”); (3) the correlation between effective vapor pressures and T_{max} of volatility groups after distinguishing isomers and thermal decomposition compounds identified by PMF (“PMF method”). The detailed description for each method and the calibration of $V_p - T_{\text{max}}$ are given in the SI.

RESULTS AND DISCUSSION

Bulk Particle Composition and Volatility. The average oxidation state of carbon (OS_C) is a metric for the degree of oxidation of organic species.⁵⁴ OS_C increases with the overall degree of oxidation. Since only C, H, and O atoms were relevant in this work, the OS_C was approximated as $\text{OS}_C = 2 \times \text{O/C} - \text{H/C}$,⁵⁴ with O/C and H/C being the ratios of oxygen and hydrogen to carbon. This simplified approach omits the existence of organic peroxides and may cause a small bias in the range of 0.1. The numbers of atoms for individual ions and

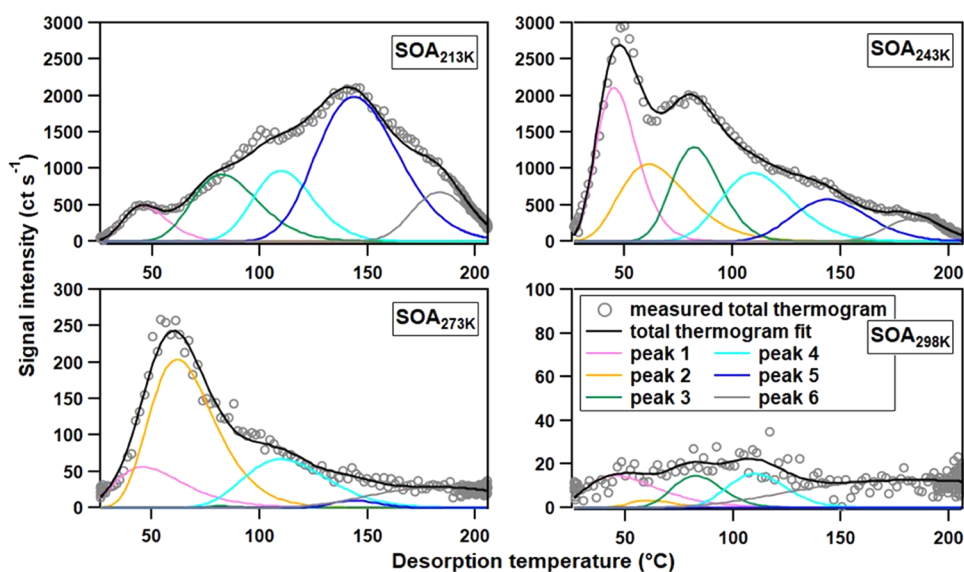


Figure 2. Fixed-peak Gaussian fit for $C_{15}H_{24}O_3I^-$ at a temperature (from top to bottom) of 213, 243, 273, and 298 K. Gray circles depict the measured data from FIGAERO-CIMS, while the black solid lines are the fitted total thermogram. Other colored solid lines show the individual compounds (fitted Gaussian peaks).

the particle bulk were assigned from the measurements from FIGAERO-CIMS and HR-AMS, respectively. The OS_C of each individual ion was weighted with its signal fraction of the total particulate organic species to obtain the average OS_C for a FIGAERO-CIMS sample.

To have an overview of the SOA bulk composition at five different temperatures, the average O/C, H/C, and OS_C for each SOA particle sample are summarized in Table S3 (SI). The average O/C from AMS measurement increased from 0.21 to 0.45 with increasing temperatures from 213 to 313 K, indicating the higher oxidation degree of SOA particles with higher temperatures. HR-AMS measurements of particles formed at 213 to 273 K appear in the region between the slope of -2 (aldehydes/ketones) and -1 (carboxylic acids) in the van-Krevelen diagram (Figure S2). This suggests that the dominant functional groups in these SOA particles were ketone/aldehyde and carboxylic acids. The OS_C of these bulk particles was less than -1 . The particles formed at 298 and 313 K had OS_C values higher than -1 and fell between the van-Krevelen slopes of -1 and 0 , indicating a higher oxygen content and the presence of alcohol/peroxy groups. This trend is supported by the molecular chemical composition of the particle phase determined by FIGAERO-CIMS (Figure S3), where the monomers (carbon atoms ≤ 15 , $C_{\leq 15}$) were detected with higher oxygen content at 298–313 K than at 213–273 K, and dimers (C_{16-30}) were only abundant at 213–243 K, as shown in Gao et al.¹¹

Figure 1 presents the mass spectra and the thermograms summed over the thermograms of all detected ions (thereafter “sum thermogram”). The sum thermograms differed in their shapes, and T_{max} values (thereafter “ $T_{max,sum}$ ”) for all SOA particles formed at varying temperatures. The $T_{max,sum}$ first decreased from 97 °C (SOA_{313K}) to 70 °C (SOA_{273K}) and then increased to 101 °C (SOA_{213K}) when the formation temperature was reduced from 313 to 213 K, also shown in Table S3 in the SI. The mass spectra show varying dominant products formed at different temperatures, indicating that the temperature dependence of chemical composition on the effective volatility of β -caryophyllene-derived SOA particles is non-

monotonic, leading to a counterintuitive behavior of $T_{max,sum}$ of the sum thermograms. The multimodal thermograms of SOA_{213K} and SOA_{243K} and the broad thermogram shapes of SOA_{273K} , SOA_{298K} , and SOA_{313K} emphasize the complexity of the β -caryophyllene SOA composition as a function of formation temperatures. This complexity of thermograms indicated that the $T_{max,sum}$ value of each sum thermogram was not necessarily representative of the overall particle volatility.

Volatility and Chemistry of a Key Monomer Ion.

$C_{15}H_{24}O_3$ is the most abundant ion for formation temperatures below 243 K. The ion thermograms are depicted in Figure 2. Two trends are visible: (1) the contribution of $C_{15}H_{24}O_3$ in both particle and gas phases decreases with increasing formation temperatures from 243 to 313 K (Figure S4) and (2) the shape of the thermograms changes significantly. The particle phase concentration at 313 K was too low to yield a meaningful thermogram shape and is thus omitted from Figure 2.

For formation temperatures higher than 273 K, the major $C_{15}H_{24}O_3$ compounds were desorbed below 100 °C during the thermal desorption. This indicates that the partitioning into the particle phase could be affected by the increasing formation temperature. However, the overall concentration of $C_{15}H_{24}O_3$ in the gas phase also decreases at formation temperatures of 273 K or above (Figure S4), which suggests that the lower concentration of particulate $C_{15}H_{24}O_3$ results mainly from the decreasing formation of $C_{15}H_{24}O_3$. It is also possible that $C_{15}H_{24}O_3$ is still formed at higher temperature but is then consumed by consecutive processes, e.g., condensed-phase reactions. The differences in the thermogram shapes for the SOA_{213K} cannot be explained by the changes in the overall concentration of $C_{15}H_{24}O_3$ but must be linked to changes in the isomeric composition and/or the ratio between monomers and oligomers.

A careful inspection of the ion thermograms shows that for each experiment at least two peaks are clearly visible in the ion thermogram and that the T_{max} of these two peaks varies between experiments. By comparing the thermograms of all

experiments, we conclude that up to six different compounds (isomers and/or decomposition products) contribute to the signal with this molecular mass or elemental composition. Hence, a set of six Gaussian peaks with manually chosen peak positions was used to fit the thermograms of $C_{15}H_{24}O_3I^-$ in all SOA samples (Figure 2), with a relative error between fitting and measured thermograms less than 2% for 243–298 K cases. Not all thermograms are composed of six modes, e.g., for SOA_{213K}, compound 2 ($T_{max} = 61$ °C) did not contribute to the fitted thermogram. This indicates that the real compound represented by compound 2 may not exist in SOA_{213K}. We acknowledge that the T_{max} values chosen for these 6 compounds will impact the fitting result. However, comparing multiple solutions with different T_{max} values showed that the overall interpretation presented below was not affected.

For $C_{15}H_{24}O_3$, compounds fitted with T_{max} below ~ 100 °C are assumed to be monomers since 100 °C is roughly the threshold temperature at which thermal decomposition may start to be relevant for carboxylic acid systems based on their estimated enthalpy of sublimation.⁵⁵ In this range, three compounds contribute significantly to the total thermogram (compound 1 ($T_{max} = 45$ °C), compound 2 ($T_{max} = 61$ °C), and compound 3 ($T_{max} = 82$ °C) in SOA_{213K} and SOA_{243K}). The observed change in the ratio between these three compounds cannot be explained by a shift toward lower volatility compounds with increasing formation temperature. Therefore, the formation pathway of the dominating isomer behind $C_{15}H_{24}O_3$ changes at varying SOA formation temperatures.

In previous studies, two isomeric compounds (β -hydroxycaryophyllon aldehyde and β -caryophyllonic acid) were identified for $C_{15}H_{24}O_3$ as early-stage oxidation products from β -caryophyllene ozonolysis.^{34,35,56,57} While it is not clear if these two compounds were indeed detected in our study, we can use these known molecular structures as examples of the types of compounds that may be produced. From the molecular structures, the expected V_p can be calculated with a group contribution method.^{58,59} V_p (298 K) of 1.4×10^{-4} Pa ($\log C_{sat}$ (298 K) of -4.8) for the aldehyde and 3.8×10^{-5} Pa ($\log C_{sat}$ (298 K) of -5.4) for the acid were estimated. Their V_p is one order of magnitude different, which shows that isomeric compounds can have distinctly different volatilities and thus have different T_{max} values during the thermal desorption.

For the higher desorption temperatures, compound 5 ($T_{max} = 144$ °C) is dominating, especially in SOA_{213K}, while it contributes less to the SOA formed at 243–298 K. Considering its T_{max} which is higher than expected for a compound with that sum formula, compound 5 is most likely a decomposition product of thermally unstable compounds with larger molecular weight, e.g., dimers or other oligomers. This suggests that the formation of dimers/oligomers, which can thermally fragment to $C_{15}H_{24}O_3$, is favored at lower SOA formation temperatures. Thermal decomposition has been found to be a significant contributor to the total ion signal in monoterpene SOA,^{48,60} and here, we suggest that it is also important in β -caryophyllene SOA. Using the calibrated correlation between V_p and T_{max} we estimate the $\log_{10} C_{298K}^*$ for these six compounds as 2.7, 2.1, 1.2, 0.1, -1.3 , and -2.8 $\mu\text{g m}^{-3}$ in order of compound number. Thus, the $C_{15}H_{24}O_3$ isomers span the LVOC and ULVOC ranges at 213–243 K and the SVOC and LVOC ranges at 273 K, while the potential decomposed oligomers are between the ULVOC and LVOC

ranges at all SOA formation temperatures, revealing a high condensing potential for β -caryophyllene oxidation products.

The presence of multiple isomers was clear for $C_{15}H_{24}O_3$ due to the distinct shape of the ion thermograms. For many other ions, it is also likely that isomers and thermal decomposition products are present, but the thermogram shapes were more difficult to interpret. Thus, manually choosing the true number of peaks and their T_{max} values became too subjective. Together with the larger number of ions in the data set, this made it infeasible to conduct a manual multipeak fit for every ion. Instead, we conducted a PMF analysis, which identifies correlations between the ion signals and can thus identify isomers or decomposition products with different volatilities within a single ion.

PMF Factors as Indicators of the SOA Formation Mechanism. A 12-factor PMF solution was chosen as the optimal solution to explain the desorption behavior of the data set with the particle samples of the five formation temperatures (Figure S5). The factor composition differs between the experiments and could be divided into three groups: cold-temperature factors, intermediate-temperature factors, and warm-temperature factors, occurring at 213–243, 243–298, and 298–313 K, respectively. The two SOA samples in the cold cases are resolved by a similar factor pattern (C1–C6) dominated by monomers (C1, C2), dimers (C3, C4, C5), and thermal decomposition compounds from oligomers (C6) based on their thermal desorption behavior and factor chemical composition, indicating similar SOA formation processes at 213–243 K. The two SOA samples in the warm case are resolved by a totally different factor pattern (W1–W3) classified in the same way as mainly monomers (W1, W2) and dimers and/or oligomers with some thermal decomposition products (W3). Note that the properties of cold-temperature factors completely differ from those of the warm-temperature factors. For example, C1 has an average composition of $C_{14.2}H_{24.0}O_{4.5}$ and a T_{max} of 60 °C, while W1 has an average composition of $C_{13.8}H_{21.4}O_{5.8}$ and a T_{max} of 85 °C, but both C1 and W1 are monomer factors. The properties of all PMF factors are described in Table 1, and the thermograms and modified Kroll diagram as well as mass spectra related to each PMF factor are shown in Figure S5. The detailed comparison of cold and warm patterns is described in the SI. The difference in factor composition between the warm and cold cases indicates the diversity of the chemical pathways and condensing processes involved in the SOA formation process in the different temperature regimes.

With varying SOA formation temperatures, PMF factors showed different responses (Figure 3). We grouped the factors according to the behavior of their signal contribution with increasing formation temperatures. “Decreasing factors” (C4, C6) showed lower contributions with increasing formation temperatures. “Increasing factors” (W2, W3) increased their contributions with formation temperatures. “Peak factors” (C1, C2, W1, I1, I2) exhibited first increasing and then decreasing contributions. “Trapezoid factors” (C3, C5) did not change their contribution between the two lowest formation temperatures, but at higher formation temperatures, their contribution decreased.

Contribution of a factor to the measured particle phase composition depends on the contribution of the compounds grouped into this factor that are produced in each experiment. The importance of individual chemical reaction pathways is temperature-dependent; e.g., the degree of autoxidation

Table 1. Summary on the Average Molecular Formula, Molecular Weight (MW), O/C, OS_C, and T_{max} of 12 PMF Factors

	factor number	molecular formula	M _W (g mol ⁻¹)	O/C	OS _C	T _{max} (°C)
cold	C1	C _{14.2} H _{24.0} O _{4.5}	266	0.35	-0.99	60
	C2	C _{14.9} H _{25.0} O _{5.6}	293	0.41	-0.85	85
	C3	C _{24.7} H _{39.4} O _{6.1}	433	0.30	-1.00	105
	C4	C _{27.3} H _{43.6} O _{5.4}	458	0.22	-1.16	95
	C5	C _{24.8} H _{39.4} O _{7.0}	449	0.34	-0.93	120
	C6	C _{28.4} H _{44.9} O _{6.5}	490	0.26	-1.08	145
warm	W1	C _{13.8} H _{21.4} O _{5.8}	280	0.45	-0.66	85
	W2	C _{15.0} H _{22.6} O _{6.8}	311	0.49	-0.53	100
	W3	C _{22.9} H _{34.0} O _{7.8}	434	0.38	-0.74	135
intermediate	I1	C _{13.5} H _{22.1} O _{5.1}	266	0.43	-0.80	70
	I2	C _{19.8} H _{31.0} O _{6.1}	366	0.34	-0.9	125
background	BG1	C _{14.3} H _{21.7} O _{5.3}	278	0.46	-0.61	N/A

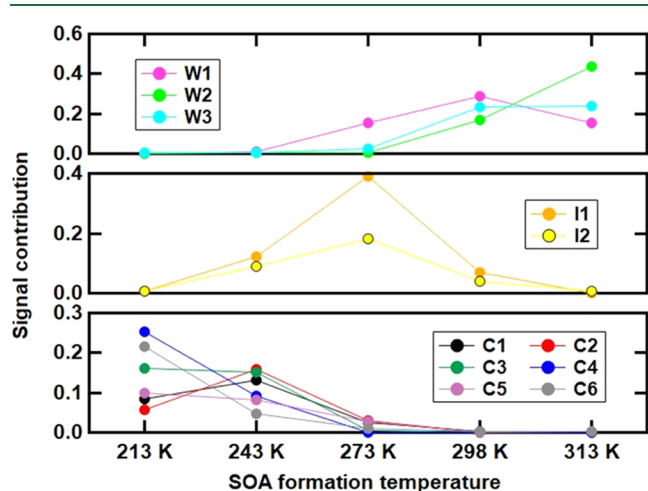


Figure 3. Factor contribution to β -caryophyllene SOA at five formation temperatures. The total detected signals are $(3.0 \pm 0.9) \times 10^4$ counts s^{-1} for each of the five samples.

increases with temperature with a signal fraction of 0.7% of HOM molecules at 213 K increasing to 9.2% at 313 K,¹¹ while dimer (C_{28–30}H_{44–48}O_{5–9}) formation was favored at 213–243 K accounting for 53.7 and 32.8% of the signal.¹¹ Hence, the particle composition is shifted toward higher oxidized compounds, which have a sufficiently low volatility at higher temperatures. Changes in the contribution of the different factors can also be caused by temperature-dependent partitioning. With higher formation temperatures, the C_‡ values of the factors increase, and the gas-to-particle phase partitioning will adjust accordingly. In other words, the compounds grouped into a factor may become too volatile to stay in the particle phase, and the contribution of this factor will decrease with increasing formation temperature.

The decreasing factors (C4, C6) only exist at 213–243 K where all compounds are estimated to be mainly in the ULVOC and ELVOC ranges (Figure 4; volatility prediction is discussed in the next section). The ELVOC and ULVOC categories can be considered to be nonvolatile and hence completely in the particle phase. Thus, the gas-to-particle partitioning did not change between 213 and 243 K and the compounds were only affected by the formation chemistry, indicating that the formation of compounds relevant to the decreasing factors was favored by low temperature. With the same reasoning, trapezoid factors also seem to be mostly governed by the formation chemistry but with a higher optimal temperature (i.e., between 213 and 243 K). Since the peak factors occur over the whole formation temperature range, both mechanisms (temperature-dependent gas-to-particle partitioning and temperature-dependent chemistry) need to be considered. As the partitioning process is expected to have a negligible impact on the factors in the ULVOC range, C1, C2, and I2 are mainly controlled by the formation chemistry with an optimal temperature of 243, 243, and 273 K, respectively. W1 falls into the LVOC (at 273 K) and SVOC ranges (at 298–313 K); thus, the partitioning to the particle phase could be reduced at the highest two formation temperatures. This counteracts the expected increase of the production of compounds grouped into W1 (i.e., HOMs), leading to a peak of the contribution at 298 K. The other two factors (W2, W3) relevant in the warm cases all have lower volatilities (ELVOC to LVOC range). They are increasing factors because the enhanced production with increasing temperature is not affected by changes in partitioning.

Therefore, we emphasize that the impact of temperature on the β -caryophyllene SOA particle formation and volatility is balanced between phase partitioning monotonically and chemical reaction pathways nonmonotonically, leading to different oxidation products existing in the particles with varying optimal temperatures.

Since the FIGAERO-CIMS data provide no direct information about the molecular structure of isomers, we cannot determine the detailed reaction pathways leading to these isomers. However, our study shows that already the β -caryophyllene-derived first-generation oxidation products can produce multiple isomers with volatilities spanning orders of magnitude. Further studies of the molecular structure of such isomers are needed to provide more details of the oxidation processes.

Volatility Determination and Comparison from Different Methods.

For all SOA samples, the volatility distributions derived from the T_{max} values of the individual ion thermograms (ion T_{max}) and the factor thermograms (factor T_{max}) are displayed in Figure 4a. The C_{298K}^{*} values are used to facilitate the comparison between samples. Using eq 2, the C_{298K}^{*} values were converted into the effective volatility class at the formation temperature, which are indicated with colored boxes in Figure 4. Generally, the volatility determined by the PMF factors is distributed at slightly lower values than the volatility derived from the ion T_{max} (Figure 4a). The shape of the distribution is similar. This is likely caused by omitting the contribution of isomers and thermal decomposition compounds when using the ion T_{max}, suggesting the potential overestimation of the volatility of particles containing a range of isomers and thermally labile compounds when using ion T_{max}.

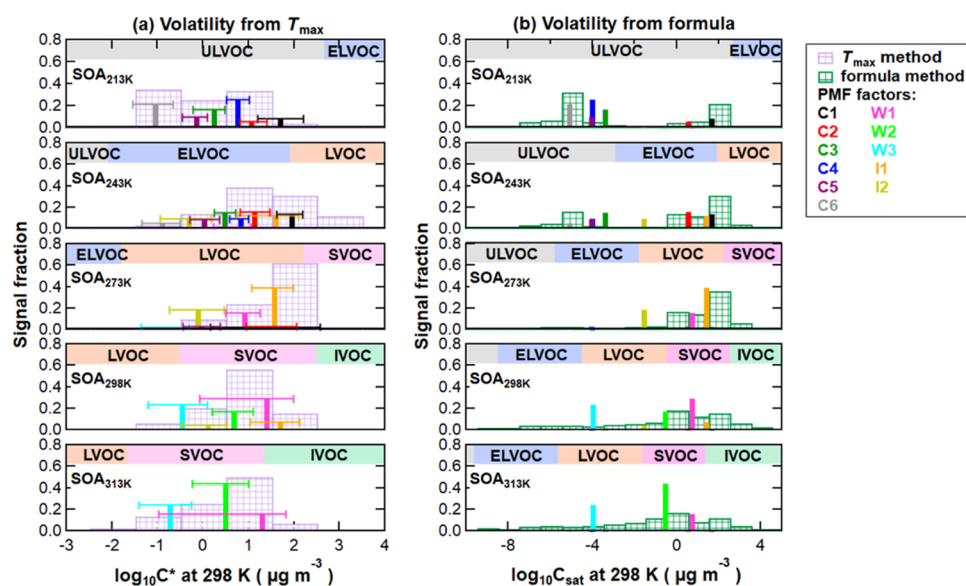


Figure 4. One-dimensional (1D) volatility basis set (1D-VBS) based on the volatility calibration (a), and formula method (b) for SOA formed at temperatures (from top to bottom) of 213, 243, 273, 298, and 313 K. Bars with green and pink grids refer to volatility derived from individual ions (individual thermogram T_{\max}), while solid sticks represent the volatility of factors from PMF analysis (average T_{\max} for each factor). Note the different x -axis ranges in panels (a, b). The colored boxes along the x -axis in panels (a, b) indicate the volatility classes:^{50,51} ULVOC, ELVOC, LVOC, SVOC, IVOC, and VOC. These boundaries of the volatility classes are defined for C_{298K}^* and are shifted to the corresponding C_{T}^* values at the formation temperatures using the Clausius–Clapeyron relation.¹²

Based on factor T_{\max} for SOA_{298K} and SOA_{313K}, all factors are in the SVOC range ($C_{298K}^* = 10^{-0.5} - 10^{1.7} \mu\text{g m}^{-3}$ for SOA_{313K}, $C_{298K}^* = 10^{-0.7} - 10^{1.3}$ for SOA_{298K}) (Figure 4a), while for SOA_{213K}, the volatility classes shift to the ULVOC range ($C_{213K}^* = 10^{-1.0} - 10^{1.7} \mu\text{g m}^{-3}$) for both monomer and dimer factors. The significantly lower formation temperatures impact the effective volatility more than the differences in chemical composition. For example, the monomer factors (C1, C2) in SOA_{213K} and SOA_{243K} have higher $\log_{10} C_{298K}^*$ than the monomeric HOM factor in SOA_{298K} and SOA_{313K} (W2). This confirms that the early-generation compounds ($\text{C}_{14.2-14.9}\text{H}_{24.0-25.0}\text{O}_{4.5-5.6}$) are more volatile than HOM species ($\text{C}_{15.0}\text{H}_{22.6}\text{O}_{6.8}$) at the same SOA formation temperatures, e.g., 298 K. However, at the lower formation temperatures, the effective volatilities of C1 and C2 in SOA_{213K} and SOA_{243K} are lower (in the ELVOC and ULVOC ranges) than those of W1 and W2 in SOA_{298K} and SOA_{313K} that are mainly in the SVOC range.

Figure 4b shows the volatility distributions derived with the formula method from the average PMF factor composition and based on the composition of the individual ions. The ion-based values spread a wider range, causing a different shape of the distribution compared with that in Figure 4a. This difference is probably caused by the grouping of ions into the PMF factors and then using the average composition. Thus, values at the upper and lower edges are included in the nearest factor and not as visible as for the individual ion case.

The differences between the formula and the T_{\max} methods originate from not only the chemical composition (e.g., activity coefficient changes)⁴⁸ in complex chemical mixtures, i.e., SOA particles, but also the existence of thermal decomposition and isomers. This is especially the case for mixtures of compounds with long carbon chains and containing a large fraction of thermally unstable oligomers. The formula method usually predicts too high volatility values because the decomposition products have less carbon and oxygen than the precursors. The

observed T_{\max} value (i.e., maximum of thermal decomposition) is lower than the theoretical T_{\max} of the precursor, leading to a volatility higher than that of the precursor but lower than the formula method value. Furthermore, the formula method assigns the same volatility to structural isomers. In contrast, the T_{\max} approach results in different volatilities for structural isomers since the T_{\max} values vary with chemical structures. Consequently, the discrepancies between the two methods vary for different temperatures because of different amounts of thermal fragments and isomers. For example, for the warmer temperatures (273–313 K), the estimated volatilities are shifted toward lower values when using the formula method. For the colder temperatures (213 and 243 K), additionally, the shape of the distribution changes. Based on the formula method, C4 and C5 have identical volatility, while their T_{\max} values suggest an order of magnitude difference.

Both the analysis of the key monomers and the PMF analysis indicate that the single ion thermogram can be created by multiple isomers and products of thermal decomposition with a range of volatilities spanning multiple orders of magnitude in C^* . Selecting a single T_{\max} value to represent the volatility of this group of compounds can work well if the group is dominated by one or a few compounds with similar volatilities and the tailing/fronting of the thermogram is not too pronounced. However, it does not account for changes in the ratio between the isomers/decomposition products and may thus overestimate the volatility of the sample.

Overall, our results indicate that the temperature influences not only the partitioning but also the chemical reaction pathways leading to different oxidation products impacting the β -caryophyllene SOA particle formation and volatility. The new volatility characterization based on the PMF analysis of thermogram data suggests that β -caryophyllene oxidation products have a high potential to nucleate aerosol particles and support their growth. Our findings show that the major formation processes for β -caryophyllene SOA vary substan-

tially, depending on the ambient temperatures (e.g., the level in the atmosphere, different seasons, and regions). Therefore, the findings of this work are improving our understanding of the formation of biogenic SOA, e.g., in atmospheric transport models. Further studies on β -caryophyllene SOA formation under other conditions, e.g., daytime chemistry, and its detailed formation mechanisms in gas (e.g., peroxy radical reactions) and particle phases, may unravel the underlying mechanistic changes in more detail.

■ ASSOCIATED CONTENT

SI Supporting Information

The Supporting Information is available free of charge at <https://pubs.acs.org/doi/10.1021/acs.est.3c01151>.

Description of the operation of the chamber, the experimental conditions, and the instrument setup for the campaign; discussion of the limitation of offline FIGAERO-CIMS analysis in this work; discussion on wall loss; description of three volatility estimation methods; volatility calibration; O/C, H/C, OS_o, and $T_{\text{max,sum}}$ of sum thermograms; van-Krevelen diagram for the bulk particles; comparison of elemental composition and oxidation from the measurements of FIGAERO-CIMS and HR-AMS; gas and particle contribution of C₁₅H₂₄O₃; description of PMF analysis of thermograms; diagnostics of PMF solution; VBS based on the formula method for monomer and oligomers; and data related to all figures, individual ions from SOA samples covering the whole temperature range, the volatility calibration, and the information related to PMF factors is openly accessible in the archive KIT (PDF)

■ AUTHOR INFORMATION

Corresponding Authors

Linyu Gao – Institute of Meteorology and Climate Research, Karlsruhe Institute of Technology, Karlsruhe 76344, Germany; Institute of Geography and Geoecology, Working Group for Environmental Mineralogy and Environmental System Analysis, Karlsruhe Institute of Technology, Karlsruhe 76131, Germany; orcid.org/0000-0001-7080-6120; Email: linyu.gao@kit.edu

Harald Saathoff – Institute of Meteorology and Climate Research, Karlsruhe Institute of Technology, Karlsruhe 76344, Germany; Email: harald.saathoff@kit.edu

Authors

Angela Buchholz – Department of Technical Physics, University of Eastern Finland, Kuopio 70210, Finland; orcid.org/0000-0002-7119-1452

Zijun Li – Department of Technical Physics, University of Eastern Finland, Kuopio 70210, Finland; International Laboratory for Air Quality and Health, School of Earth and Atmospheric Sciences, Queensland University of Technology, Brisbane, QLD 4001, Australia; orcid.org/0000-0002-2973-1216

Junwei Song – Institute of Meteorology and Climate Research, Karlsruhe Institute of Technology, Karlsruhe 76344, Germany; Institute of Geography and Geoecology, Working Group for Environmental Mineralogy and Environmental System Analysis, Karlsruhe Institute of Technology, Karlsruhe 76131, Germany

Magdalena Vallon – Institute of Meteorology and Climate Research, Karlsruhe Institute of Technology, Karlsruhe 76344, Germany

Feng Jiang – Institute of Meteorology and Climate Research, Karlsruhe Institute of Technology, Karlsruhe 76344, Germany; Institute of Geography and Geoecology, Working Group for Environmental Mineralogy and Environmental System Analysis, Karlsruhe Institute of Technology, Karlsruhe 76131, Germany

Ottmar Möhler – Institute of Meteorology and Climate Research, Karlsruhe Institute of Technology, Karlsruhe 76344, Germany

Thomas Leisner – Institute of Meteorology and Climate Research, Karlsruhe Institute of Technology, Karlsruhe 76344, Germany; Institute of Environmental Physics, Heidelberg University, Heidelberg 69120, Germany

Complete contact information is available at: <https://pubs.acs.org/doi/10.1021/acs.est.3c01151>

Notes

The authors declare no competing financial interest.

■ ACKNOWLEDGMENTS

This work was supported by H2020 European Research Council (CHAPAs (grant no. 850614)). L.G., J.S., and F.J. acknowledge the China Scholarship Council (CSC) for financial support and the Graduate School for Climate and Environment (GRACE). The authors thank Dr. Yuxuan Bian for his technical help in manually fitting of thermograms and the IMK-AAF technicians at the KIT for their support of this work.

■ REFERENCES

- (1) Fehsenfeld, F.; Calvert, J.; Fall, R.; Goldan, P.; Guenther, A. B.; Hewitt, C. N.; Lamb, B.; Liu, S.; Trainer, M.; Westberg, H.; Zimmerman, P. Emissions of volatile organic compounds from vegetation and the implications for atmospheric chemistry. *Global Biogeochem. Cycles* **1992**, *6*, 389–430.
- (2) Mellouki, A.; Wallington, T. J.; Chen, J. Atmospheric Chemistry of Oxygenated Volatile Organic Compounds: Impacts on Air Quality and Climate. *Chem. Rev.* **2015**, *115*, 3984–4014.
- (3) Laothawornkitkul, J.; Taylor, J. E.; Paul, N. D.; Hewitt, C. N. Biogenic volatile organic compounds in the Earth system. *New Phytol.* **2009**, *183*, 27–51.
- (4) Charnawskas, J. C.; Alpert, P. A.; Lambe, A. T.; Berkemeier, T.; O'Brien, R. E.; Massoli, P.; Onasch, T. B.; Shiraiwa, M.; Moffet, R. C.; Gilles, M. K.; Davidovits, P.; Worsnop, D. R.; Knopf, D. A. Condensed-phase biogenic–anthropogenic interactions with implications for cold cloud formation. *Faraday Discuss.* **2017**, *200*, 165–194.
- (5) Kroll, J. H.; Seinfeld, J. H. Chemistry of secondary organic aerosol: Formation and evolution of low-volatility organics in the atmosphere. *Atmos. Environ.* **2008**, *42*, 3593–3624.
- (6) Bianchi, F.; Kurtén, T.; Riva, M.; Mohr, C.; Rissanen, M. P.; Roldin, P.; Berndt, T.; Crouse, J. D.; Wennberg, P. O.; Mentel, T. F.; Wildt, J.; Junninen, H.; Jokinen, T.; Kulmala, M.; Worsnop, D. R.; Thornton, J. A.; Donahue, N.; Kjaergaard, H. G.; Ehn, M. Highly Oxygenated Organic Molecules (HOM) from Gas-Phase Autoxidation Involving Peroxy Radicals: A Key Contributor to Atmospheric Aerosol. *Chem. Rev.* **2019**, *119*, 3472–3509.
- (7) Carlton, A. G.; Wiedinmyer, C.; Kroll, J. H. A review of Secondary Organic Aerosol (SOA) formation from isoprene. *Atmos. Chem. Phys.* **2009**, *9*, 4987–5005.
- (8) Donahue, N. M.; Epstein, S. A.; Pandis, S. N.; Robinson, A. L. A two-dimensional volatility basis set: 1. organic-aerosol mixing thermodynamics. *Atmos. Chem. Phys.* **2011**, *11*, 3303–3318.

- (9) Praplan, A. P.; Schobesberger, S.; Bianchi, F.; Rissanen, M. P.; Ehn, M.; Jokinen, T.; Junninen, H.; Adamov, A.; Amorim, A.; Dommen, J.; Duplissy, J.; Hakala, J.; Hansel, A.; Heintritz, M.; Kangasluoma, J.; Kirkby, J.; Krapf, M.; Kürten, A.; Lehtipalo, K.; Riccobono, F.; Rondo, L.; Sarnela, N.; Simon, M.; Tomé, A.; Tröstl, J.; Winkler, P. M.; Williamson, C.; Ye, P.; Curtius, J.; Baltensperger, U.; Donahue, N. M.; Kulmala, M.; Worsnop, D. R. Elemental composition and clustering behaviour of α -pinene oxidation products for different oxidation conditions. *Atmos. Chem. Phys.* **2015**, *15*, 4145–4159.
- (10) Frege, C.; Ortega, I. K.; Rissanen, M. P.; Praplan, A. P.; Steiner, G.; Heinritzi, M.; Ahonen, L.; Amorim, A.; Bernhammer, A. K.; Bianchi, F.; Brilke, S.; Breitenlechner, M.; Dada, L.; Dias, A.; Duplissy, J.; Ehrhart, S.; El-Haddad, I.; Fischer, L.; Fuchs, C.; Garmash, O.; Gonin, M.; Hansel, A.; Hoyle, C. R.; Jokinen, T.; Junninen, H.; Kirkby, J.; Kürten, A.; Lehtipalo, K.; Leiminger, M.; Mauldin, R. L.; Molteni, U.; Nichman, L.; Petäjä, T.; Sarnela, N.; Schobesberger, S.; Simon, M.; Sipilä, M.; Stolzenburg, D.; Tomé, A.; Vogel, A. L.; Wagner, A. C.; Wagner, R.; Xiao, M.; Yan, C.; Ye, P.; Curtius, J.; Donahue, N. M.; Flagan, R. C.; Kulmala, M.; Worsnop, D. R.; Winkler, P. M.; Dommen, J.; Baltensperger, U. Influence of temperature on the molecular composition of ions and charged clusters during pure biogenic nucleation. *Atmos. Chem. Phys.* **2018**, *18*, 65–79.
- (11) Gao, L.; Song, J.; Mohr, C.; Huang, W.; Vallon, M.; Jiang, F.; Leisner, T.; Saathoff, H. Kinetics, SOA yields and chemical composition of secondary organic aerosol from β -caryophyllene ozonolysis with and without nitrogen oxides between 213 and 313 K. *Atmos. Chem. Phys. Discuss.* **2022**, *22*, 6001–6020.
- (12) Ye, Q.; Wang, M.; Hofbauer, V.; Stolzenburg, D.; Chen, D.; Schervish, M.; Vogel, A.; Mauldin, R. L.; Baalbaki, R.; Brilke, S.; Dada, L.; Dias, A.; Duplissy, J.; El Haddad, I.; Finkenzeller, H.; Fischer, L.; He, X.; Kim, C.; Kürten, A.; Lamkaddam, H.; Lee, C. P.; Lehtipalo, K.; Leiminger, M.; Manninen, H. E.; Marten, R.; Mentler, B.; Partoll, E.; Petäjä, T.; Rissanen, M.; Schobesberger, S.; Schuchmann, S.; Simon, M.; Tham, Y. J.; Vazquez-Pufleau, M.; Wagner, A. C.; Wang, Y.; Wu, Y.; Xiao, M.; Baltensperger, U.; Curtius, J.; Flagan, R.; Kirkby, J.; Kulmala, M.; Volkamer, R.; Winkler, P. M.; Worsnop, D.; Donahue, N. M. Molecular Composition and Volatility of Nucleated Particles from α -Pinene Oxidation between -50 °C and $+25$ °C. *Environ. Sci. Technol.* **2019**, *53*, 12357–12365.
- (13) Buchholz, A.; Ylisirniö, A.; Huang, W.; Mohr, C.; Canagaratna, M.; Worsnop, D. R.; Schobesberger, S.; Virtanen, A. Deconvolution of FIGAERO–CIMS thermal desorption profiles using positive matrix factorisation to identify chemical and physical processes during particle evaporation. *Atmos. Chem. Phys.* **2020**, *20*, 7693–7716.
- (14) Tikkanen, O. P.; Buchholz, A.; Ylisirniö, A.; Schobesberger, S.; Virtanen, A.; Yli-Juuti, T. Comparing secondary organic aerosol (SOA) volatility distributions derived from isothermal SOA particle evaporation data and FIGAERO–CIMS measurements. *Atmos. Chem. Phys.* **2020**, *20*, 10441–10458.
- (15) Li, Z.; Buchholz, A.; Ylisirniö, A.; Barreira, L.; Hao, L.; Schobesberger, S.; Yli-Juuti, T.; Virtanen, A. Evolution of volatility and composition in sesquiterpene-mixed and α -pinene secondary organic aerosol particles during isothermal evaporation. *Atmos. Chem. Phys.* **2021**, *21*, 18283–18302.
- (16) Atkinson, R.; Arey, J. Atmospheric Degradation of Volatile Organic Compounds. *Chem. Rev.* **2003**, *103*, 4605–4638.
- (17) Arangio, A. M.; Tong, H.; Socorro, J.; Pöschl, U.; Shiraiwa, M. Quantification of environmentally persistent free radicals and reactive oxygen species in atmospheric aerosol particles. *Atmos. Chem. Phys.* **2016**, *16*, 13105–13119.
- (18) Lopez-Hilfiker, F. D.; Mohr, C.; Ehn, M.; Rubach, F.; Kleist, E.; Wildt, J.; Mentel, T. F.; Lutz, A.; Hallquist, M.; Worsnop, D.; Thornton, J. A. A novel method for online analysis of gas and particle composition: description and evaluation of a Filter Inlet for Gases and AEROSols (FIGAERO). *Atmos. Meas. Tech.* **2014**, *7*, 983–1001.
- (19) Bannan, T. J.; Le Breton, M.; Priestley, M.; Worrall, S. D.; Bacak, A.; Marsden, N. A.; Mehra, A.; Hammes, J.; Hallquist, M.; Alfara, M. R.; Krieger, U. K.; Reid, J. P.; Jayne, J.; Robinson, W.; McFiggans, G.; Coe, H.; Percival, C. J.; Topping, D. A method for extracting calibrated volatility information from the FIGAERO-HR-ToF-CIMS and its experimental application. *Atmos. Meas. Tech.* **2019**, *12*, 1429–1439.
- (20) Thornton, J. A.; Mohr, C.; Schobesberger, S.; D'Ambro, E. L.; Lee, B. H.; Lopez-Hilfiker, F. D. Evaluating Organic Aerosol Sources and Evolution with a Combined Molecular Composition and Volatility Framework Using the Filter Inlet for Gases and Aerosols (FIGAERO). *Acc. Chem. Res.* **2020**, *53*, 1415–1426.
- (21) Paatero, P.; Tapper, U. Positive matrix factorization: A non-negative factor model with optimal utilization of error estimates of data values. *Environmetrics* **1994**, *5*, 111–126.
- (22) Barreira, L. M. F.; Ylisirniö, A.; Pullinen, I.; Buchholz, A.; Li, Z.; Lipp, H.; Junninen, H.; Hörrak, U.; Noe, S. M.; Krasnova, A.; Krasnov, D.; Kask, K.; Talts, E.; Niinemets, Ü.; Ruiz-Jimenez, J.; Schobesberger, S. The importance of sesquiterpene oxidation products for secondary organic aerosol formation in a springtime hemiboreal forest. *Atmos. Chem. Phys.* **2021**, *21*, 11781–11800.
- (23) Xu, L.; Pye, H. O. T.; He, J.; Chen, Y.; Murphy, B. N.; Ng, N. L. Experimental and model estimates of the contributions from biogenic monoterpenes and sesquiterpenes to secondary organic aerosol in the southeastern United States. *Atmos. Chem. Phys.* **2018**, *18*, 12613–12637.
- (24) Faiola, C. L.; Buchholz, A.; Kari, E.; Yli-Pirilä, P.; Holopainen, J. K.; Kivimäenpää, M.; Miettinen, P.; Worsnop, D. R.; Lehtinen, K. E. J.; Guenther, A. B.; Virtanen, A. Terpene Composition Complexity Controls Secondary Organic Aerosol Yields from Scots Pine Volatile Emissions. *Sci. Rep.* **2018**, *8*, No. 3053.
- (25) Hellén, H.; Praplan, A. P.; Tykkä, T.; Ylivinkka, I.; Vakkari, V.; Bäck, J.; Petäjä, T.; Kulmala, M.; Hakola, H. Long-term measurements of volatile organic compounds highlight the importance of sesquiterpenes for the atmospheric chemistry of a boreal forest. *Atmos. Chem. Phys.* **2018**, *18*, 13839–13863.
- (26) Li, H.; Canagaratna, M. R.; Riva, M.; Rantala, P.; Zhang, Y.; Thomas, S.; Heikkinen, L.; Flaud, P. M.; Villenave, E.; Perraudin, E.; Worsnop, D.; Kulmala, M.; Ehn, M.; Bianchi, F. Atmospheric organic vapors in two European pine forests measured by a Vocus PTR-TOF: insights into monoterpene and sesquiterpene oxidation processes. *Atmos. Chem. Phys.* **2021**, *21*, 4123–4147.
- (27) Maclean, A. M.; Smith, N. R.; Li, Y.; Huang, Y.; Hettiyadura, A. P. S.; Crescenzo, G. V.; Shiraiwa, M.; Laskin, A.; Nizkorodov, S. A.; Bertram, A. K. Humidity-Dependent Viscosity of Secondary Organic Aerosol from Ozonolysis of β -Caryophyllene: Measurements, Predictions, and Implications. *ACS Earth Space Chem.* **2021**, *5*, 305–318.
- (28) Yee, L. D.; Isaacman-VanWertz, G.; Wernis, R. A.; Meng, M.; Rivera, V.; Kreisberg, N. M.; Hering, S. V.; Bering, M. S.; Glasius, M.; Upshur, M. A.; Gray Bé, A.; Thomson, R. J.; Geiger, F. M.; Offenberg, J. H.; Lewandowski, M.; Kourtchev, I.; Kalberer, M.; de Sá, S.; Martin, S. T.; Alexander, M. L.; Palm, B. B.; Hu, W.; Campuzano-Jost, P.; Day, D. A.; Jimenez, J. L.; Liu, Y.; McKinney, K. A.; Artaxo, P.; Viegas, J.; Manzi, A.; Oliveira, M. B.; de Souza, R.; Machado, L. A. T.; Longo, K.; Goldstein, A. H. Observations of sesquiterpenes and their oxidation products in central Amazonia during the wet and dry seasons. *Atmos. Chem. Phys.* **2018**, *18*, 10433–10457.
- (29) Fouqueau, A.; Cirtog, M.; Cazaunau, M.; Panguit, E.; Doussin, J. F.; Picquet-Varrault, B. An experimental study of the reactivity of terpinolene and β -caryophyllene with the nitrate radical. *Atmos. Chem. Phys.* **2022**, *22*, 6411–6434.
- (30) Khan, M. A. H.; Jenkin, M. E.; Foulds, A.; Derwent, R. G.; Percival, C. J.; Shallcross, D. E. A modeling study of secondary organic aerosol formation from sesquiterpenes using the STOCHEM global chemistry and transport model. *J. Geophys. Res.: Atmos.* **2017**, *122*, 4426–4439.
- (31) Ding, X.; He, Q.-F.; Shen, R.-Q.; Yu, Q.-Q.; Wang, X.-M. Spatial distributions of secondary organic aerosols from isoprene, monoterpene, β -caryophyllene, and aromatics over China during summer. *J. Geophys. Res.: Atmos.* **2014**, *119*, 11,877–11,891.

- (32) Hellén, H.; Praplan, A. P.; Tykkä, T.; Helin, A.; Schallhart, S.; Schiestl-Aalto, P. P.; Bäck, J.; Hakola, H. Sesquiterpenes and oxygenated sesquiterpenes dominate the VOC (C₅–C₂₀) emissions of downy birches. *Atmos. Chem. Phys.* **2021**, *21*, 8045–8066.
- (33) Kesselmeier, J.; Staudt, M. Biogenic Volatile Organic Compounds (VOC): An Overview on Emission, Physiology and Ecology. *J. Atmos. Chem.* **1999**, *33*, 23–88.
- (34) Winterhalter, R.; Herrmann, F.; Kanawati, B.; Nguyen, T. L.; Peeters, J.; Vereecken, L.; Moortgat, G. K. The gas-phase ozonolysis of β -caryophyllene (C₁₅H₂₄). Part I: an experimental study. *Phys. Chem. Chem. Phys.* **2009**, *11*, 4152–4172.
- (35) Li, Y. J.; Chen, Q.; Guzman, M. I.; Chan, C. K.; Martin, S. T. Second-generation products contribute substantially to the particle-phase organic material produced by β -caryophyllene ozonolysis. *Atmos. Chem. Phys.* **2011**, *11*, 121–132.
- (36) Geron, C. D.; Arnsts, R. R. Seasonal monoterpene and sesquiterpene emissions from *Pinus taeda* and *Pinus virginiana*. *Atmos. Environ.* **2010**, *44*, 4240–4251.
- (37) Jardine, K.; Serrano, A. Y.; Arneith, A.; Abrell, L.; Jardine, A.; van Haren, J.; Artaxo, P.; Rizzo, L. V.; Ishida, F. Y.; Karl, T.; Kesselmeier, J.; Saleska, S.; Huxman, T. Within-canopy sesquiterpene ozonolysis in Amazonia. *J. Geophys. Res.: Atmos.* **2011**, *116*, No. 301.
- (38) Möhler, O.; Stetzer, O.; Schaefer, S.; Linke, C.; Schnaiter, M.; Tiede, R.; Saathoff, H.; Krämer, M.; Mangold, A.; Budz, P.; Zink, P.; Schreiner, J.; Mauersberger, K.; Haag, W.; Kärcher, B.; Schurath, U. Experimental investigation of homogeneous freezing of sulphuric acid particles in the aerosol chamber AIDA. *Atmos. Chem. Phys.* **2003**, *3*, 211–223.
- (39) Wagner, R.; Bunz, H.; Linke, C.; Möhler, O.; Naumann, K.-H.; Saathoff, H.; Schnaiter, M.; Schurath, U. In *Chamber Simulations of Cloud Chemistry: The AIDA Chamber*; Springer: Netherlands: Dordrecht, 2006; Vol. 2006, pp 67–82.
- (40) Lopez-Hilfiker, F. D.; Iyer, S.; Mohr, C.; Lee, B. H.; D'Ambro, E. L.; Kurtén, T.; Thornton, J. A. Constraining the sensitivity of iodide adduct chemical ionization mass spectrometry to multifunctional organic molecules using the collision limit and thermodynamic stability of iodide ion adducts. *Atmos. Meas. Tech.* **2016**, *9*, 1505–1512.
- (41) Canagaratna, M. R.; Jimenez, J. L.; Kroll, J. H.; Chen, Q.; Kessler, S. H.; Massoli, P.; Hildebrandt Ruiz, L.; Fortner, E.; Williams, L. R.; Wilson, K. R.; Surratt, J. D.; Donahue, N. M.; Jayne, J. T.; Worsnop, D. R. Elemental ratio measurements of organic compounds using aerosol mass spectrometry: characterization, improved calibration, and implications. *Atmos. Chem. Phys.* **2015**, *15*, 253–272.
- (42) Aiken, A. C.; DeCarlo, P. F.; Kroll, J. H.; Worsnop, D. R.; Huffman, J. A.; Docherty, K. S.; Ulbrich, I. M.; Mohr, C.; Kimmel, J. R.; Sueper, D.; Sun, Y.; Zhang, Q.; Trimborn, A.; Northway, M.; Ziemann, P. J.; Canagaratna, M. R.; Onasch, T. B.; Alfarra, M. R.; Prevot, A. S. H.; Dommen, J.; Duplissy, J.; Metzger, A.; Baltensperger, U.; Jimenez, J. L. O/C and OM/OC Ratios of Primary, Secondary, and Ambient Organic Aerosols with High-Resolution Time-of-Flight Aerosol Mass Spectrometry. *Environ. Sci. Technol.* **2008**, *42*, 4478–4485.
- (43) <https://cires1.colorado.edu/jimenez-group/ToFAMSResources/ToFSoftware/index.html>.
- (44) Lanz, V. A.; Alfarra, M. R.; Baltensperger, U.; Buchmann, B.; Hueglin, C.; Prévôt, A. S. H. Source apportionment of submicron organic aerosols at an urban site by factor analytical modelling of aerosol mass spectra. *Atmos. Chem. Phys.* **2007**, *7*, 1503–1522.
- (45) Jimenez, J. L.; Canagaratna, M. R.; Donahue, N. M.; Prevot, A. S. H.; Zhang, Q.; Kroll, J. H.; DeCarlo, P. F.; Allan, J. D.; Coe, H.; Ng, N. L.; Aiken, A. C.; Docherty, K. S.; Ulbrich, I. M.; Grieshop, A. P.; Robinson, A. L.; Duplissy, J.; Smith, J. D.; Wilson, K. R.; Lanz, V. A.; Hueglin, C.; Sun, Y. L.; Tian, J.; Laaksonen, A.; Raatikainen, T.; Rautiainen, J.; Vaattovaara, P.; Ehn, M.; Kulmala, M.; Tomlinson, J. M.; Collins, D. R.; Cubison, M. J.; Dunlea, J.; Huffman, J. A.; Onasch, T. B.; Alfarra, M. R.; Williams, P. I.; Bower, K.; Kondo, Y.; Schneider, J.; Drewnick, F.; Borrmann, S.; Weimer, S.; Demerjian, K.; Salcedo, D.; Cottrell, L.; Griffin, R.; Takami, A.; Miyoshi, T.; Hatakeyama, S.; Shimono, A.; Sun, J. Y.; Zhang, Y. M.; Dzepina, K.; Kimmel, J. R.; Sueper, D.; Jayne, J. T.; Herndon, S. C.; Trimborn, A. M.; Williams, L. R.; Wood, E. C.; Middlebrook, A. M.; Kolb, C. E.; Baltensperger, U.; Worsnop, D. R. Evolution of Organic Aerosols in the Atmosphere. *Science* **2009**, *326*, 1525–1529.
- (46) Ulbrich, I. M.; Canagaratna, M. R.; Zhang, Q.; Worsnop, D. R.; Jimenez, J. L. Interpretation of organic components from Positive Matrix Factorization of aerosol mass spectrometric data. *Atmos. Chem. Phys.* **2009**, *9*, 2891–2918.
- (47) Donahue, N. M.; Robinson, A. L.; Stanier, C. O.; Pandis, S. N. Coupled Partitioning, Dilution, and Chemical Aging of Semivolatile Organics. *Environ. Sci. Technol.* **2006**, *40*, 2635–2643.
- (48) Stark, H.; Yatavelli, R. L. N.; Thompson, S. L.; Kang, H.; Krechmer, J. E.; Kimmel, J. R.; Palm, B. B.; Hu, W.; Hayes, P. L.; Day, D. A.; Campuzano-Jost, P.; Canagaratna, M. R.; Jayne, J. T.; Worsnop, D. R.; Jimenez, J. L. Impact of Thermal Decomposition on Thermal Desorption Instruments: Advantage of Thermogram Analysis for Quantifying Volatility Distributions of Organic Species. *Environ. Sci. Technol.* **2017**, *51*, 8491–8500.
- (49) Epstein, S. A.; Riipinen, I.; Donahue, N. M. A Semiempirical Correlation between Enthalpy of Vaporization and Saturation Concentration for Organic Aerosol. *Environ. Sci. Technol.* **2010**, *44*, 743–748.
- (50) Donahue, N. M.; Robinson, A. L.; Pandis, S. N. Atmospheric organic particulate matter: From smoke to secondary organic aerosol. *Atmos. Environ.* **2009**, *43*, 94–106.
- (51) Schervish, M.; Donahue, N. M. Peroxy radical chemistry and the volatility basis set. *Atmos. Chem. Phys.* **2020**, *20*, 1183–1199.
- (52) Li, Y.; Pöschl, U.; Shiraiwa, M. Molecular corridors and parameterizations of volatility in the chemical evolution of organic aerosols. *Atmos. Chem. Phys.* **2016**, *16*, 3327–3344.
- (53) Ylisirniö, A.; Barreira, L. M. F.; Pullinen, I.; Buchholz, A.; Jayne, J.; Krechmer, J. E.; Worsnop, D. R.; Virtanen, A.; Schobesberger, S. On the calibration of FIGAERO-ToF-CIMS: importance and impact of calibrant delivery for the particle-phase calibration. *Atmos. Meas. Tech.* **2021**, *14*, 355–367.
- (54) Kroll, J. H.; Donahue, N. M.; Jimenez, J. L.; Kessler, S. H.; Canagaratna, M. R.; Wilson, K. R.; Altieri, K. E.; Mazzoleni, L. R.; Wozniak, A. S.; Bluhm, H.; Mysak, E. R.; Smith, J. D.; Kolb, C. E.; Worsnop, D. R. Carbon oxidation state as a metric for describing the chemistry of atmospheric organic aerosol. *Nat. Chem.* **2011**, *3*, 133–139.
- (55) Salo, K.; Jonsson, A.; Andersson, P.; Hallquist, M. Aerosol Volatility and Enthalpy of Sublimation of Carboxylic Acids. *J. Phys. Chem. A* **2010**, *114*, 4586–4594.
- (56) Jaoui, M.; Leungakul, S.; Kamens, R. M. Gas and Particle Products Distribution from the Reaction of β -Caryophyllene with Ozone. *J. Atmos. Chem.* **2003**, *45*, 261–287.
- (57) Chan, M. N.; Surratt, J. D.; Chan, A. W. H.; Schilling, K.; Offenberg, J. H.; Lewandowski, M.; Edney, E. O.; Kleindienst, T. E.; Jaoui, M.; Edgerton, E. S.; Tanner, R. L.; Shaw, S. L.; Zheng, M.; Knipping, E. M.; Seinfeld, J. H. Influence of aerosol acidity on the chemical composition of secondary organic aerosol from β -caryophyllene. *Atmos. Chem. Phys.* **2011**, *11*, 1735–1751.
- (58) Moller, B.; Rarey, J.; Ramjugernath, D. Estimation of the vapour pressure of non-electrolyte organic compounds via group contributions and group interactions. *J. Mol. Liq.* **2008**, *143*, 52–63.
- (59) Nannoolal, Y.; Rarey, J.; Ramjugernath, D.; Cordes, W. Estimation of pure component properties: Part 1. Estimation of the normal boiling point of non-electrolyte organic compounds via group contributions and group interactions. *Fluid Phase Equilib.* **2004**, *226*, 45–63.
- (60) Docherty, K. S.; Wu, W.; Lim, Y. B.; Ziemann, P. J. Contributions of Organic Peroxides to Secondary Aerosol Formed from Reactions of Monoterpenes with O₃. *Environ. Sci. Technol.* **2005**, *39*, 4049–4059.